

Aharonov-Bohm effect in a side-gated graphene ring

M. Huefner ^{*,†}, F. Molitor^{*}, A. Jacobsen, A. Pioda, K. Ensslin, and T. Ihn
Solid State Physics Laboratory, ETH Zurich, Switzerland

C. Stampfer

JARA-FIT and II. Institute of Physics, RWTH Aachen, Germany

(Dated: November 15, 2021)

We investigate the magnetoresistance of a side-gated ring structure etched out of single-layer graphene. We observe Aharonov-Bohm oscillations with about 5% visibility. We are able to change the relative phases of the wave functions in the interfering paths and induce phase jumps of π in the Aharonov-Bohm oscillations by changing the voltage applied to the side gate or the back gate. The observed data can be interpreted within existing models for 'dirty metals' giving a phase coherence length of the order of 1 μm at a temperature of 500 mK.

PACS numbers:

The progress in nano-fabrication technology of graphene has led to the realization of graphene constrictions^{1,2,3,4,5,6} and quantum dots.^{7,8,9,10} The same technology allows one to study phase coherent transport of charge carriers in single- and multilayer graphene. In Ref. 11, weak localization and conductance fluctuations in mesoscopic samples with about seven graphene layers were investigated. Recent transport measurements on single-layer pnp- (nnp-) junctions created with a narrow top gate were interpreted in terms of Fabry-Perot interference.¹² Magnetoconductance fluctuations and weak localization effects were observed in single-layers with superconducting contacts.^{13,14} Theoretical aspects of phase-coherent conductance fluctuations in graphene nanostructures,¹⁵ and the Aharonov-Bohm effect^{16,17} have been addressed.^{18,19}

The Aharonov-Bohm effect has been observed in carbon-materials i.e. carbon nanotubes before^{20,21}. Recently the Aharonov-Bohm effect was investigated experimentally in two-terminal graphene ring structures, and a systematic study of its dependence on temperature, density of charge carriers, and magnetic field was presented.²² In this experiment the visibility of the Aharonov-Bohm oscillations was found to be less than 1% at low magnetic fields. It was speculated that this small value might be due to inhomogeneities in the two interferometer arms leading to a tunneling constriction that suppressed the oscillations.

In this paper we present four-terminal magnetotransport through a side-gated graphene ring of smaller size than the devices studied in Ref. 22, and demonstrate h/e -periodic Aharonov-Bohm oscillations with a visibility of more than 5%. In addition, we demonstrate that a π -phase shift of the oscillations can be achieved by changing the side or back gate voltages.

Fig. 1(a) displays a scanning force micrograph of the graphene ring studied in this work. The graphene

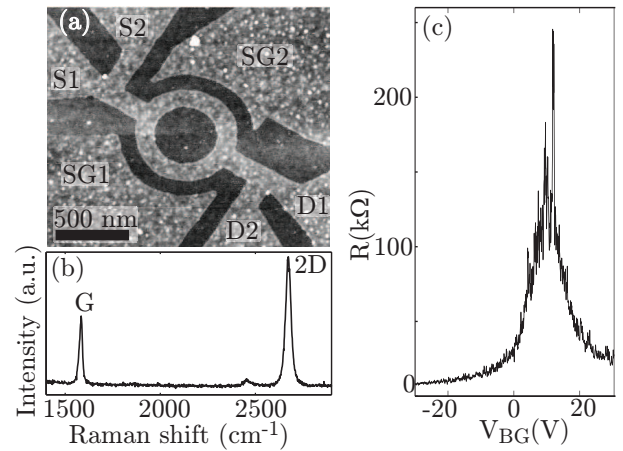


FIG. 1: (a) Scanning force micrograph of the ring structure studied in this work. The ring has an inner radius of about 200 nm and an outer radius of about 350 nm. On each end of the ring structure, there are two graphene contact pads labeled S1/2 and D1/2 allowing us to perform four-terminal resistance measurements. The side gates labeled SG1 and SG2 are located 100 nm away from the structure. (b) Raman spectrum of the same flake before processing. The spectrum was recorded using a laser excitation wavelength of 532 nm. (c) Four-terminal resistance across the ring structure as a function of back gate voltage, with both side gates grounded. The measurement is recorded at a temperature of 500 mK with a constant current of 10 nA.

flakes are produced by mechanical exfoliation of natural graphite, and deposited on a highly doped Si wafer covered by 295 nm of silicon dioxide.²³ Thin flakes are detected by optical microscopy, and Raman spectroscopy is used to confirm the single layer nature of the selected graphitic flakes.^{24,25} In Fig. 1(b) we show the Raman spectrum of the investigated graphene ring device [Fig. 1(a)]. The spectrum has been recorded before structuring the flake and the narrow, single Lorentzian shape of the 2D line is evidence for the single layer nature.^{24,25} Electron beam lithography, followed by reactive ion etching is used to

^{*}Both authors have contributed equally to this work.

define the structure. The contacts are added in a second electron beam lithography step, followed by the evaporation of Cr/Au (2 nm/40 nm).⁸

All measurements presented in this work are performed in a He³ cryostat at a base temperature of $T \approx 500$ mK. Standard low-frequency lock-in techniques are used to measure the resistance by applying a constant current. A magnetic field is applied perpendicular to the sample plane.

Fig. 1(c) displays the four-terminal resistance of the ring as a function of applied back gate voltage V_{BG} . The charge neutrality point occurs at $V_{BG} \approx 10$ V. The high resistance observed at the charge neutrality point is related to the small width $W = 150$ nm of the ring arms.⁵ However, this width was chosen large enough that strong localization of charge carriers leading to Coulomb-blockade dominated transport in narrow ribbons^{5,6} is not dominant. A rough estimate of the mobility taking into account the geometry of the structure and using the parallel plate capacitor model leads to $\mu \approx 5000$ cm²/Vs, comparable to the value quoted for the material used in Ref. 22. For the typical back gate voltage $V_{BG} = -5.8$ V used for most of the measurements presented in this paper, the parallel plate capacitor model gives the sheet carrier density $p_s = 1.2 \times 10^{12}$ cm⁻².

We identify the relevant transport regime in terms of appropriate length scales. The Fermi wavelength corresponding to the carrier density mentioned above is $\lambda_F = \sqrt{4\pi/p_s} = 33$ nm. For comparison, at the same density the mean free path is $l = \hbar\mu\sqrt{\pi p_s}/e \approx 65$ nm. This is less than half of the width W of the arms, and much smaller than the mean ring radius $r_0 = 275$ nm and its corresponding circumference $L = 1.7$ μ m. Therefore, the presented measurements are all close to the diffusive (dirty metal) regime, and carrier scattering at the sample boundaries alone cannot fully account for the value of the mean free path. The relevance of thermal averaging of phase-coherent effects can be judged from the thermal length $l_{th} = \hbar v_F l / 2k_B T = 700$ nm, which is significantly smaller than L . This indicates that thermal averaging of interference contributions to the conductance is expected to be relevant.

Fig. 2(a) displays the four-terminal resistance of the ring as a function of magnetic field at $V_{BG} = -5.789$ V. The raw data trace shows a strong modulation of the background resistance on a magnetic field scale of about 100 mT. Clear periodic oscillations can be seen on top of this background. They have a period in magnetic field $\Delta B_{AB} = 17.9$ mT, indicated by the vertical lines. This period corresponds to the h/e -periodic Aharonov-Bohm oscillations of a ring structure of 271 nm radius, in good agreement with the mean radius r_0 of the ring.

Fig. 2(b) shows the same data with the background resistance subtracted. The background was determined by performing a running average over one Aharonov-Bohm period ΔB_{AB} . This method was found to lead to no relevant distortion of the oscillations after background subtraction (with some exception in Fig. 3 around $B = 0$ T,

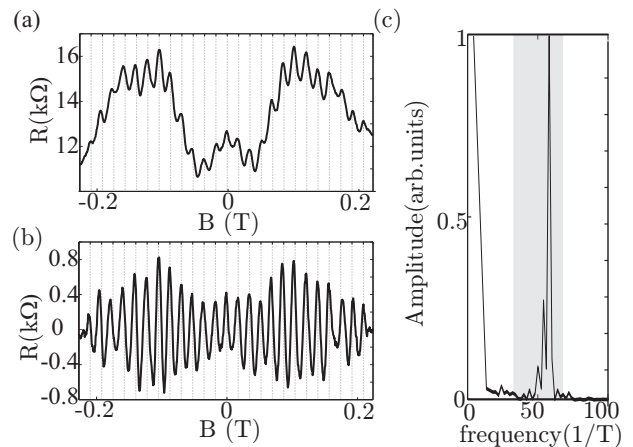


FIG. 2: Four-terminal resistance across the ring as a function of magnetic field, recorded at $V_{BG} = -5.789$ V with a constant current of 5 nA. (a) displays the raw data. For figure (b), the background resistance has been subtracted as described in the text. (c) Fourier transform of the trace.

which is of minor importance for this paper.) The amplitude of the Aharonov-Bohm oscillations is modulated as a function of magnetic field on the same scale as the background resistance, indicating that a finite number of paths enclosing a range of different areas contribute to the oscillations. This observation is compatible with the finite width W of the ring.²⁹

In Fig. 2(c) the fast Fourier transform (FFT) of the data in Fig. 2(a) is plotted. The peak seen at 60 mT corresponds to the h/e -periodic Aharonov-Bohm effect. The width of this peak is significantly smaller than the range of frequencies expected from the range of possible enclosed areas in our geometry (indicated as a gray shaded region in Fig. 2(c)). We therefore conclude that the paths contributing to the Aharonov-Bohm effect do not cover the entire geometric area of the ring arms.

In this four-terminal measurement, the oscillations have a visibility of about 5%. In general, the observed Aharonov-Bohm oscillations become more pronounced for smaller current levels, as expected. The current level of 5 nA was chosen as a good compromise between the signal-to-noise ratio of the voltage measurement and the visibility of the Aharonov-Bohm oscillations. However, due to limited sample stability, the visibility of the oscillations at a given back gate voltage depends on the back gate voltage history. Therefore measurements presented here were taken only over small ranges of back gate voltage after having allowed the sample to stabilize in this range.

Higher harmonics, especially $h/2e$ -periodic oscillations, are neither visible in the magnetoresistance traces, nor do they lead to a clear peak in the Fourier spectrum (less than 1% of the h/e -oscillation amplitude). This indicates that the phase coherence length $l_\varphi < 2L$, i.e., it is (significantly) smaller than twice the circumference of the ring. Given the temperature of our experiment, this esti-

mate is well compatible with the phase-coherence lengths reported in Refs. 11, 13, 22, and 30.

The measurements were taken in a magnetic field range where the classical cyclotron radius $R_c = \hbar k_F / eB > 640$ nm is bigger than the mean free path l , the ring width W , and even the ring diameter. At the same time, Landau level quantization effects are negligible, because the sample is studied in the low field regime $\mu B \ll 1$. The only relevant effect of the magnetic field on the charge carrier dynamics is therefore caused by the field-induced Aharonov–Bohm phase.

In diffusive ring-shaped systems, conductance fluctuations can coexist with Aharonov–Bohm oscillations. However, the relevant magnetic field scale of the conductance fluctuations $\Delta B_{CF} \sim \phi_0 / W l_\varphi$ ($\phi_0 = h/e$) can be forced to be well separated from $\Delta B_{AB} = \phi_0 / \pi r_0^2$ by choosing a sufficiently large aspect ratio r_0 / W . Judging the situation from the measurement traces in Fig. 2(a), the only candidates for conductance fluctuations are the magnetic field dependent variations of the background resistance, which occur on a magnetic field scale that is at least a factor of five larger than ΔB_{AB} . As far as the amplitude of the modulation of the background can be estimated from Fig. 2(a), it is of the order of the conductance quantum e^2/h which is reasonable, since the condition $l_\varphi \sim L$ implies the absence of strong self-averaging over the ring circumference L .

Fig. 3 displays the four-terminal resistance of the ring as a function of magnetic field and voltage V_{SG} applied to the side gate SG1, for two different back gate voltages without [Fig. 3(a), (c)] and with [Fig. 3(b), (d)] background subtraction. In the raw data [Fig. 3(a), (c)], a modulation of the background resistance on a magnetic field scale, similar to that in Fig. 2(a), can be observed. The subtraction of the background (extracted as described before) makes the Aharonov–Bohm oscillations visible [Fig. 3(b), (d)]. Aharonov–Bohm oscillations at different V_{SG} display either a minimum or a maximum at $B = 0$ T, with abrupt changes between the two cases at certain side gate voltage values. This behavior is compatible with the generalized Onsager symmetry requirement for two-terminal resistance measurements, $R(B) = R(-B)$. Although our measurement has been performed in four-terminal configuration, the contact arrangement with respect to the ring and the fact, that the contacts are separated by distances $\geq l_\varphi$ from the ring lead to a setup where the two terminal symmetry is still very strong. [c.f., Fig. 1(a)]. Closer inspection shows that the part antisymmetric in magnetic field of each trace (not shown) is more than a factor of ten smaller than the symmetric part.

In previous studies on metal rings the effect of electric fields on the Aharonov–Bohm oscillations has been investigated, and two possible scenarios were discussed:³¹ on one hand, the electric field may shift electron paths in space and thereby change the interference. On the other hand, the electric field may change the electron density and thereby the Fermi-wavelength of the carriers. We

discuss the latter effect in more detail below, since the relative change in the Fermi wavelength is expected to be more pronounced in graphene compared to conventional metals.

In order to estimate which phase change $\Delta\varphi$ an electronic wave picks up on the scale of the side gate voltage change ΔV_{SG} on which Aharonov–Bohm maxima switch to minima, we use the relation $\Delta\varphi = \Delta k_F L_{\text{eff}}$, where L_{eff} , being the effective length of a characteristic diffusive path, is assumed to be independent of the side gate voltage,³² whereas the change in wave number Δk_F is assumed to be caused by ΔV_{SG} . The quantity Δk_F is found from the density change Δp_s using $\Delta k_F = \sqrt{\pi/4p_s} \Delta p_s$. The density change is related via a parallel plate capacitor model to a change in back gate voltage, i.e., $\Delta p_s = \Delta V_{BG} \epsilon \epsilon_0 / ed$ (ϵ : relative dielectric constant of the silicon dioxide substrate, d : thickness of the oxide layer) leading to $\Delta p_s / \Delta V_{BG} \approx 7.5 \times 10^{10} \text{ cm}^{-2} \text{ V}^{-1}$. Finally, ΔV_{BG} is related to ΔV_{SG} via the lever arm ratio $\alpha_{SG} / \alpha_{BG}$.

In order to determine this lever arm ratio, we have performed measurements of conductance fluctuations in the plane of the back gate voltage V_{BG} and the side gate voltage V_{SG} (not shown). The characteristic slope of fluctuation minima and maxima in this parameter plane allows us to estimate the lever arm ratio $\alpha_{SG} / \alpha_{BG} \approx 0.2$. In previous experiments on side-gated graphene Hall bars³³ we found a similar lever arm for regions close to the edge of the Hall bar whose width is roughly comparable to the width of the arms of the ring investigated here.

Using the numbers given above and using the density $p_s = 1.2 \times 10^{12} \text{ cm}^{-2}$ for Fig. 3(b), we find $\Delta k_F \approx 1.2 \times 10^6 \text{ m}^{-1} \text{ V}^{-1} \Delta V_{SG}$. In ballistic systems the effective length of a path is given by $L_{\text{eff}} \sim L$, giving $\Delta\varphi \approx \Delta V_{SG} \pi / 1.5 \text{ V}$. A phase change of π would imply a change of side gate voltage on the scale of 1.5 V which is large compared with the measurement in Fig. 3(b) where this scale is of the order of 100 mV. However, in the diffusive regime, a characteristic path contributing to Aharonov–Bohm oscillations is longer by a factor of $L/l \approx 27$ due to multiple scattering³⁴ giving $\Delta\varphi \approx \Delta V_{SG} \pi / 55 \text{ mV}$. A change of the side gate voltage of typically 55 mV would cause a switch of the Aharonov–Bohm phase by π , in better agreement with the observation than the ballistic estimate. The same calculation could be used to estimate the correlation voltage of the conductance fluctuations of the background resistance, in agreement with the observation in Fig. 2 and Fig. 3. This correlation voltage is on the same scale as the phase jumps of the Aharonov–Bohm oscillations.

Fig. 4 shows magnetoresistance data for varying back gate voltages and $V_{SG} = 0 \text{ V}$. Similar to the case where the side gate was tuned, we observe variations of the oscillation patterns as well as π -phase shifts. The raw data displayed in Fig. 4(a),- shows background fluctuations with h/e -periodic Aharonov–Bohm oscillations superimposed. In Fig. 4(b), the background has been removed. Again, alternating minima and maxima at $B = 0$ T can

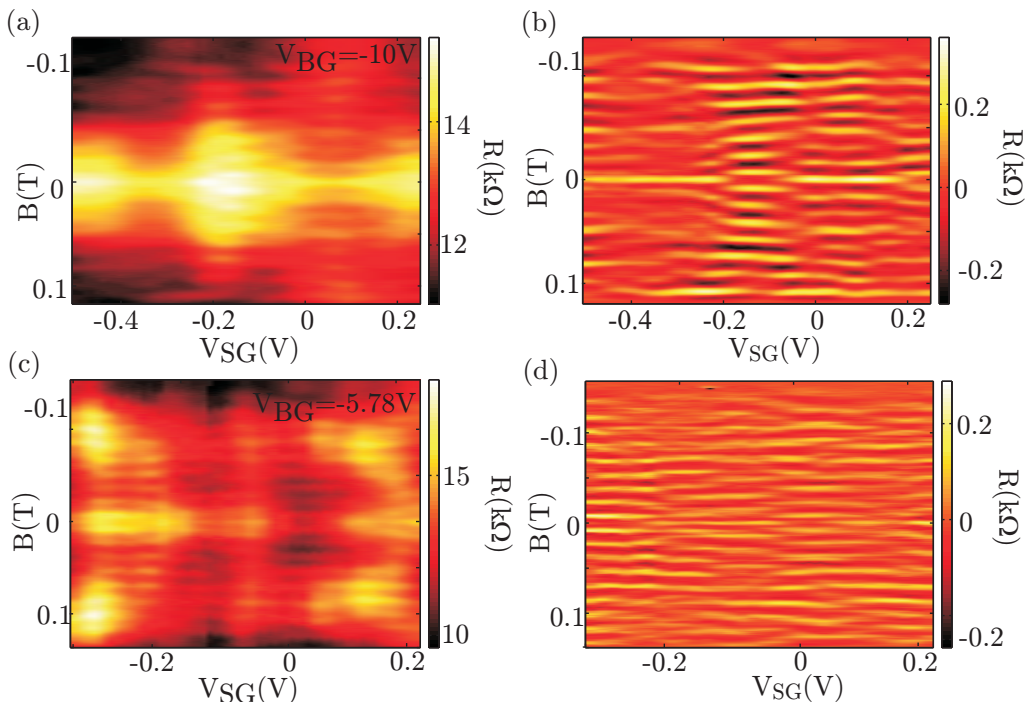


FIG. 3: Four-terminal resistance as a function of magnetic field B and voltage applied to SG1 (V_{SG}), measured with a constant current $I = 1$ nA. (a) and (c) show the raw data, recorded at $V_{BG} = -10$ V and $V_{BG} = -5.789$ V. Figures (b) and (d) show the corresponding data where the background has been removed for each individual trace by averaging over one Aharonov–Bohm period in magnetic field.

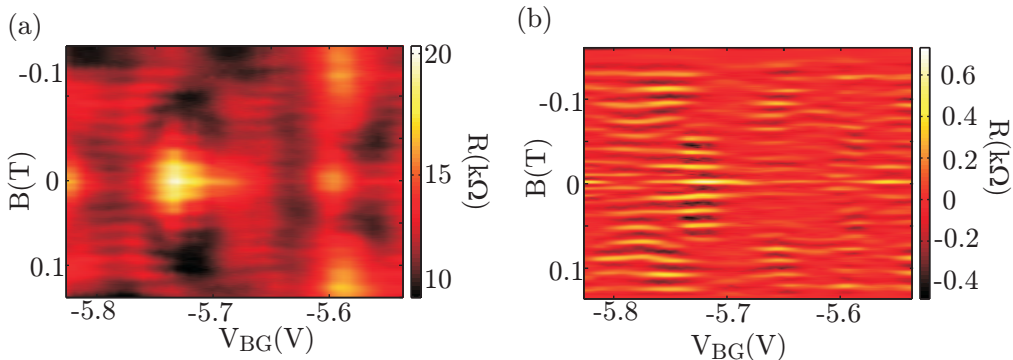


FIG. 4: Four-terminal resistance as a function of magnetic field and back gate voltage measured with a constant current of 1 nA. (a) displays the raw data, while for (b) the background has been removed.

be observed.

The larger visibility of Aharonov–Bohm oscillations observed in our sample, compared to the work in Ref. 22 is unlikely to be caused by better material or sample quality. Also our measurement temperature is about a factor of four higher than the lowest temperatures reported there. We therefore believe that the smaller ring dimensions in combination with the four terminal arrangement may be responsible for the larger value of the visibility observed in our experiment. In Ref. 22 the expression²⁹ $\Delta G \propto l_{th}/l_\varphi \exp(-\pi r_0/l_\varphi)$ was invoked to explain the observed $T^{-1/2}$ -dependence of the oscillation amplitude. The exponential term on the right hand side contains

the radius of the ring r_0 . A smaller radius will lead to a larger oscillation amplitude which may explain the improved amplitude in our measurements. However, trying to relate the visibilities observed in the two experiments quantitatively (assuming that all experimental parameters except the ring radius are the same) would lead to a phase-coherence length l_φ smaller than the ring circumference L and only slightly larger than the ring radius r_0 . As our experiment demonstrates, a separation of h/e -periodic oscillations from background variations due to magnetoconductance fluctuations is still possible in our device despite the aspect ratio r_0/W which is reduced in our device compared to Ref. 22. A phase-coherence

length between L and r_0 is also compatible with the observation $\Delta B_{CF}/\Delta B_{AB} \approx 5$.

We also note that the diffusive regime investigated in our device is quite extended in back gate voltage. Assuming diffusive scattering at the edges to become dominant as soon as $l \approx W$, we estimate that this does not occur (for transport in the valence band) until V_{BG} becomes more negative than -80 V. Transport may also enter a different regime, when the Fermi wavelength becomes larger than l , which is expected to happen (again for transport in the valence band) at back-gate voltages larger than $+2$ V in our sample. An even different regime may be entered at a back gate voltage of $+9.3$ V, where $\lambda_F \approx W$. As a consequence, the ‘dirty metal’ description of the Aharonov–Bohm oscillations should be applicable in the whole range of back-gate voltages shown in Fig. 1(c), except for a region of ± 8 V around the charge neutrality point, where the resistance is maximum.

In conclusion, we have observed Aharonov–Bohm os-

cillations in four-terminal measurements on a side-gated graphene ring structure. The visibility of the oscillations is found to be about 5%. By changing the voltage applied to the lateral side gate, or the back gate, we observe phase jumps of π compatible with the generalized Onsager relations for two-terminal measurements. The observations are in good agreement with an interpretation in terms of diffusive metallic transport in a ring geometry, and a phase-coherence length of the order of one micrometer at a temperature of 500 mK.

Acknowledgments

Support by the ETH FIRST lab and financial support by the EH Zuerich and from the Swiss Science Foundation (Schweizerischer Nationalfonds, NCCR Nanoscience) are gratefully acknowledged.

[†] Electronic address: huefner@phys.ethz.ch

- ¹ M. Y. Han, B. Ozyilmaz, Y. Zhang, and P. Kim, *Phys. Rev. Lett.* **98**, 206805 (2007).
- ² Z. Chen, Y.-M. Lin, M. J. Rooks, and P. Avouris, *Physica E*, **40/2**, 228 (2007).
- ³ X. Liu, J. B. Oostinga, A. F. Morpurgo, L. M.K. Vandersypen, *Phys. Rev. B* **80**, 121407(R), (2009).
- ⁴ K. Todd, H. Chou, S. Amasha and D. Goldhaber-Gordon, *Nano Lett.*, **9**,1 (2009).
- ⁵ F. Molitor, A. Jacobsen, C. Stampfer, J. Güttinger, T. Ihn, and K. Ensslin *Phys. Rev. B* **79**, 075426 (2009).
- ⁶ C. Stampfer, J. Güttinger, S. Hellmüller, F. Molitor, K. Ensslin, and T. Ihn, *Phys. Rev. Lett.* **102**, 056403 (2009).
- ⁷ L. A. Ponomarenko, F. Schedin, M. I. Katsnelson, R. Yang, E. H. Hill, K. S. Novoselov, A. K. Geim, *Science*, **320**, 356 (2008)
- ⁸ C. Stampfer, J. Güttinger, F. Molitor, D. Graf, T. Ihn and K. Ensslin, *Appl. Phys. Lett* **92**, 012102 (2008);
- ⁹ C. Stampfer, E. Schurtenberger, F. Molitor, J. Güttinger, T. Ihn and K. Ensslin, *Nano. Lett.* **8**, 2378 (2008)
- ¹⁰ S. Schnez, F. Molitor, C. Stampfer, J. Güttinger, I. Shorubalko, T. Ihn and K. Ensslin, *Appl. Phys. Lett.* **94**, 012107 (2009)
- ¹¹ D. Graf, F. Molitor, T. Ihn, K. Ensslin, *Phys. Rev. B* **75**, 245429 (2007).
- ¹² A. F. Young and P. Kim, *Nature Physics* **5**, 222 (2009).
- ¹³ F. Miao, S. Wijeratne, Y. Zhang, U. C. Coskun, W. Bao and C. N. Lau, *Science* **317**, 1530 (2007)
- ¹⁴ H. B. Heersche, P. Jarillo-Herrero, J. B. Oostinga, L. M. K. Vandersypen and A. F. Morpurgo, *Nature* **446**, 56 (2007)
- ¹⁵ A. Rycerz, J. Tworzynski, C.W.J. Beenakker, *Europhys. Lett.* **79**, 57003 (2007).
- ¹⁶ Y. Aharonov and D. Bohm, *Phys. Rev.* **115**, 485 (1959)
- ¹⁷ R. A. Webb, S. Washburn, C. P. Umbach and R. B. Laibowith, *Phys. Rev. Lett.* **54**, 2696 (1985)
- ¹⁸ P. Recher, B. Trauzettel, A. Rycerz, Ya.M. Blanter, C.W.J. Beenakker, A.F. Morpurgo, *Phys. Rev. B* **76**, 235404 (2007).
- ¹⁹ A. Rycerz, *Acta Physica Polonica A* **115**, 322 (2009).

- ²⁰ A. Bachtold et al., *Nature* **397**, 673 (1999).
- ²¹ J. Cao et al., *Phys. Rev. Lett.* **93**, 216803 (2004).
- ²² S. Russo, J. B. Oostinga, D. Wehenkel, H. B. Heersche, S. Shams Sobhani, L. M. K. Vandersypen and A. F. Morpurgo, *Phys. Rev. B* **77**, 085413 (2008).
- ²³ K. S. Novoselov, A. K. Geim, S. V. Morozov, D. Jiang, Y. Zhang, S. V. Dubonos, I. V. Grigorieva, and A. A. Firsov, *Science* **306**, 666 (2004)
- ²⁴ A. C. Ferrari, J. C. Meyer, V. Scardaci, C. Casiraghi, M. Lazzeri, F. Mauri, S. Piscanec, D. Jiang, K. S. Novoselov, S. Roth, and A. K. Geim, *Phys. Rev. Lett.* **97**, 187401 (2006)
- ²⁵ D. Graf, F. Molitor, K. Ensslin, C. Stampfer, A. Jungen, C. Hierold, and L. Wirtz, *Nano Lett.* **7**, 238 (2007)
- ²⁶ L. Onsager, *Phys. Rev.* **37**, 405 (1931)
- ²⁷ L. Onsager, *Phys. Rev.* **38**, 2265 (1931)
- ²⁸ M. Büttiker, *Phys. Rev. Lett.* **57**, 1761 (1986)
- ²⁹ S. Washburn, R.A. Webb, *Adv. Phys.* **35**, 375 (1986).
- ³⁰ C. Berger *et al.*, *Science* **312**, 1191 (2006).
- ³¹ S. Washburn, H. Schmid, D. Kern, and R. A. Webb, *Phys. Rev. Lett.* **59**, 1791 (1987); P. G. N. de Vegvar, G. Timp, P. M. Mankiewich, R. Behringer, and J. Cunningham, *Phys. Rev. B* **40**, 3491 (1989).
- ³² We remark here that this assumption, and the reasoning based on it as given in the main text, corresponds to the usual argument made for dirty metals. However, in graphene the typical length $L_{\text{eff}} = L^2/l$ of a diffusive path³⁴ is proportional to k_F^{-1} , such that the phase $k_F L_{\text{eff}}$ accumulated along such a path is independent of k_F and therefore independent of carrier density and gate voltage. It therefore remains unclear to us, how the concept of the Thouless energy as an energy scale for wave function correlations can be transferred to the graphene system. We nevertheless discuss the estimate based on the assumption of a k_F -independent L_{eff} (1) in the absence of any better theory and (2) in accordance with Ref. 22.
- ³³ F. Molitor, J. Güttinger, C. Stampfer, D. Graf, T. Ihn and K. Ensslin, *Phys. Rev. B* **76**, 245426 (2007)
- ³⁴ Y. Imry, *Introduction to mesoscopic physics*, 2nd ed., p.

73, Oxford University Press, New York, 2002.